JOURNAL OF MATERIALS SCIENCE **34** (1999) 4181–4191

Optimizing energy absorption in multi-layered materials through controlled delamination

M. H. LEAR
Test Engineer, 46th Test Wing, Eglin AFB, FL, USA

B. V. SANKAR
Professor, Aerospace Engineering, Mechanics & Engineering Science, University of Florida, USA

The intent of this paper is to investigate the mechanics of delamination growth in an isotropic, ideally-brittle layered material under an impact load and to present guidelines for the design of more energy absorbent structures. Using a finite element model, both two- and three-layered configurations are considered. Prompted by the results from this model, closed-form solutions for the interlaminar shear strength and the interfacial fracture toughness corresponding to maximum energy absorption are derived for the two-layered laminate. These solutions were used to develop guidelines for the optimal design of two- and three-layered laminates.

1. Introduction

Since the beginning of the modern transportation era, a need has existed for effective protection against impact. Most of the techniques currently employed focus on damage tolerance or the ability to maintain residual strength after impact occurs. Because delaminations in layered beams greatly reduce residual strength, it is usually beneficial to minimize their extent. For many applications this is appropriate, since most structures, especially those in the aerospace industry, must be able to sustain numerous minor impacts before needing repair.

Recently, several researchers [1–4] have recognized that the extent of delamination in layered materials can profoundly affect the amount of energy absorbed during impact. Based upon this concept, the focus of impact protection may be switched from maintaining residual strength to using the formation of delaminations to maximize energy absorption. While this concept is appealing, it does leave the structure with low residual strength and, consequently makes it vulnerable to future impacts. If, instead, a disposable barrier-shell designed specifically for damage protection is wrapped around the structure, the shell may be removed and replaced after it is damaged, leaving the interior undamaged and intact. Such impact bumpers could also be applied as cheap modifications to existing structures, perhaps in a manner similar to the tiles that form the heat shield on the space shuttle.

Many industries already employ barrier-shells for impact energy absorption. Race car bodies are designed to crush and peal off, each piece taking a bit of the impact's kinetic energy with it, saving the rigid driver chassis from harm. Tanks also employ similar layering techniques to protect against missile strikes. Recent work [1] has also hinted at using metallic layered materials for automobile bumpers and highway guard rails. Unfortunately, design guidelines for using damage formation as a mechanism for energy absorption have not yet been established. This study was designed to explore the mechanics of delamination in layered materials in order to establish such guidelines for achieving optimal energy absorption.

In the present study, a layered beam under a statically applied three-point bending load was considered. Static loading has previously been found to be a good approximation for low velocity impact when the impactor mass is large compared to that of the beam [5].

2. Model

2.1. Structure

Since the focus of this work was on the benefits of layering, failure was assumed to occur in the interface alone. Thus, transverse (tensile) failure of the lamina was considered catastrophic and represented final failure. In order to isolate the effect of interface delamination upon the absorbed energy, only two- and three-layer geometries as shown in Fig. 1 were considered.

A finite element model with twenty-four Euler-Bernoulli beam elements was used to represent the brittle lamina. This number gave excellent agreement with standard solutions (i.e., 3-point bend and end-notched flexure). The simulation of an adhesive interface was accomplished with Lagrange's method of undetermined multipliers. This is a simple yet powerful means of enforcing constraints without the numerical problems associated with stiff springs. In matrix form, the constraints may be written as $[C]\{u\} = \{0\}$, where $[C]$ is a constraint matrix, $\{u\}$ is the displacement vector, and $\{0\}$ is the null vector.

Because of the offset created by not having the beam nodes collocated along the interface, the coupling

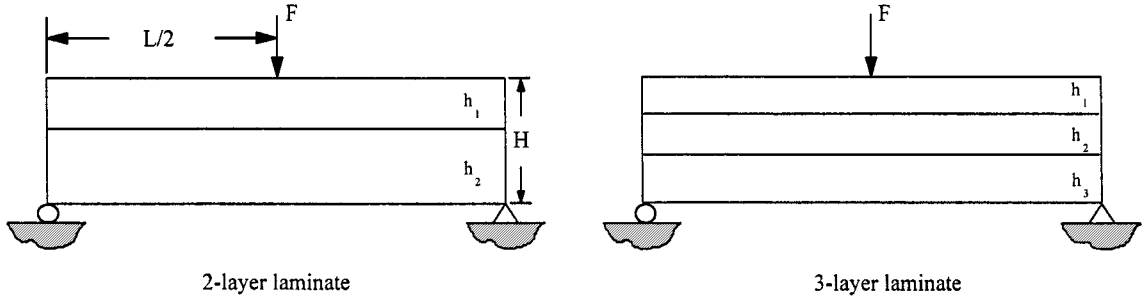

Figure 1 Specimen geometry.

between the rotational and translational dof. must be accounted for. If small rotations are assumed, the rotational effect on the vertical (v) displacement may be neglected, but the horizontal (u) component constraint becomes,

$$u_1 - \left(\frac{h_1}{2}\right)\theta_1 = u_2 + \left(\frac{h_2}{2}\right)\theta_2$$

where u_1, h_1, and θ_1 refer to the top beam node and u_2, h_2, and θ_2 refer to the bottom beam node.

Putting these constraints into matrix form, $[C]$ is found.

$$C = \begin{bmatrix} 1 & 0 & -h_1/2 & -1 & 0 & -h_2/2 \\ 0 & 1 & 0 & 0 & -1 & 0 \\ 0 & 0 & 1 & 0 & 0 & -1 \end{bmatrix}$$

From this a rigid element stiffness matrix can be determined by the relation,

$$k = \begin{bmatrix} 0 & C^{\mathrm{T}} \\ C & 0 \end{bmatrix}$$

2.2. Crack propagation

Because brittle behavior is assumed in both the lamina and interface materials, Griffith's [6] strain energy release rate criteria may be used to predict the onset of crack propagation in lieu of the more tedious stress field analysis. The basic equation for the strain energy release rate, G, is given in Equation 1, below.

$$G = \frac{\partial U}{\partial A} \tag{1}$$

With this method, the fracture mechanics failure criterion is $G \geq G_{\mathrm{c}}$. It is important to note that there are actually three modes of fracture—opening (I), shearing (II), and tearing (III); however, since transverse failure of the lamina was the final failure criteria, the crack growth is purely Model II. For this reason, G_{II} and $G_{\mathrm{II_c}}$ (the Mode II energy release rates) will be referred to simply as G and G_{c}.

Two methods were used for the calculation of the strain energy release rate: Virtual Crack Extension and the Zero Volume Integral. The Virtual Crack Extension method directly applies Equation 1. The Zero Volume Integral method is based on the J-integral concept developed by Rice [7]. Because of its numerical efficiency and accuracy, the Zero Volume Integral method was used in the simpler two-layer case, but for reasons to be explained below, it could not be used for three-layer laminates. For this configuration, the Virtual Crack Extension method had to be employed.

Virtual Crack Extension is the most basic and the most commonly used method for the calculation of G. As stated above, it relies on the direct application of Equation 1 in the numerical model. When displacement control and the force-displacement relation are applied, the strain energy release rate becomes,

$$G = \frac{1}{2}\{u\}^{\mathrm{T}}\left\{\frac{\partial F}{\partial A}\right\} \tag{2}$$

where $\{u\}$ and $\{F\}$ are the displacement and load vectors along the midspan. In the finite element model, the derivative in Equation 2 can be computed numerically using forward difference. Thus, the crack is propagated a small amount, ΔA (i.e., one element) and a load change, ΔF, is found. This method proved to be very useful with three-layered laminates where the Zero Volume Integral couldn't be applied. Unfortunately, it was comparatively computationally expensive and slightly less accurate due to the numerical differentiation.

The Zero Volume Integral developed by Shankar [8] to model delaminations in composite beams and later [9] composite plates afforded a tremendous savings in computational effort.

Since this method uses already calculated values (i.e., loads and displacements), the extra "virtual" propagation step in the Virtual Crack Extension method was not required. As long as the beam elements around the crack tip are chosen such that the x-directional cosines and the top and bottom surface tractions are zero, the J-integral, and hence, the strain energy release rate, for a two-layered laminate, degenerates to the following,

$$G = 1/b\left(U_{\mathrm{L}}^{(1)} + U_{\mathrm{L}}^{(4)} - U_{\mathrm{L}}^{(2)} - U_{\mathrm{L}}^{(3)}\right) \tag{3}$$

where b is the width of the laminate and the $U_{\mathrm{L}}^{(i)}$'s are the strain energy densities (strain energy per unit length) of the respective beam sections as shown in Fig. 2.

In a three-layer beam where both interfaces have started to delaminate, Equation 3 may be applied to each crack tip.

$$G_1 = 1/b\left(U_{\mathrm{L}}^{(4)} + U_{\mathrm{L}}^{(5)} - U_{\mathrm{L}}^{(3)} - U_{\mathrm{L}}^{(6)}\right)$$

$$G_2 = 1/b\left(U_{\mathrm{L}}^{(1)} + U_{\mathrm{L}}^{(4)} - U_{\mathrm{L}}^{(2)} - U_{\mathrm{L}}^{(3)}\right)$$

G_1 and G_2 represent for the top and bottom crack, respectively. This result implies that all of the energy in the middle layer (elements 3 and 4) contributes equally to both cracks—an obvious violation of the

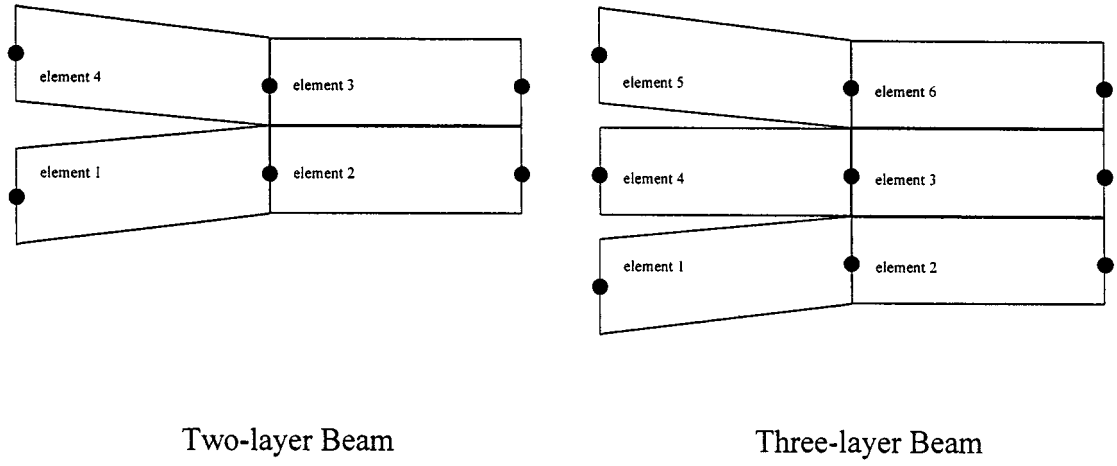

Figure 2 Zero-volume path for calculating J.

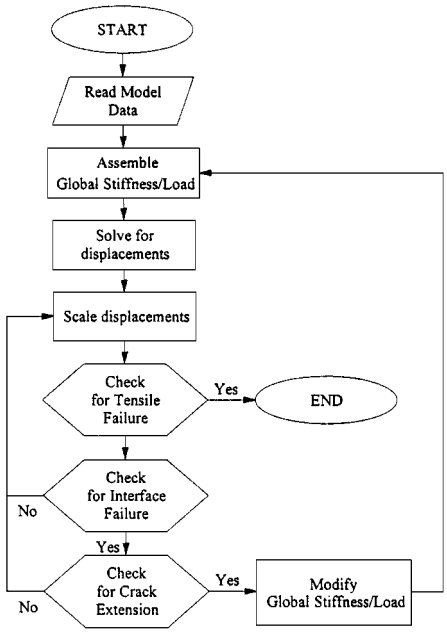

Figure 3 Algorithm flow diagram.

conservation of energy principle. Certainly, some fraction of $U_L^{(3)}$ and $U_L^{(4)}$ apply to each crack, but isolating the portions is not a simple matter. Thus, for three-layer beams only the Virtual Crack Extension method was used.

2.3. Algorithm

A basic flow diagram for the finite element model used is given in Fig. 3.

Since load and displacement are linearly related, it was not necessary to solve the system at each loading increment. Instead, a Green's function calculation routine was used in order to save computer effort. Thus, during the "Solve for displacements" procedure, a unit displacement was applied and the total system response was measured. This response was then "scaled" in the "Scale displacements" phase to reflect the true loading state. The displacements resulting from this stage were used to calculate forces and stresses.

The tensile bending stresses were calculated from the basic beam theory combined stress formula. Shear stresses along the undelaminated interfaces were calculated assuming a parabolic variation through the thickness. In three-layer laminate cases where only one interface had failed, the delaminated interface was considered a free surface and separate shear distributions were found for the sections above and below the delamination. It was assumed that once the interface failed due to shear, an initial crack of length (a_0) formed and that further crack propagation was governed by the strain energy release criteria described above. The creation of this initial crack has been previously documented [5] and is considered a reasonable assumption.

The Green's function technique worked as long as no change in the stiffness matrix or load vector occurred. When the interface failed or the crack propagated, the global stiffness matrix and load vector were recompiled and the system was resolved as shown in the "Modify Global Stiffness/Load" block and return loop. The "new" system went through the Green's function process again until it too failed.

3. Optimal interfacial properties

The first set of finite element tests were designed to establish the relationship between the interfacial properties (shear strength and fracture toughness) and energy absorption. In order to isolate the effect of property changes, a single interface system (i.e., two-layer) like that shown in Fig. 1 was used.

3.1. Optimal interfacial shear strength

Several trials were run for various combinations of shear strength and fracture toughness. For each layer thickness configuration the results of these tests were compiled into Energy vs. Shear Strength plots; however, since all of the results followed a similar trend only the optimal case ($h_1 = h_2$) is presented (Figs 4 and 6). The data was found to be discontinuous due to a change in the final failure mechanism, and was, thus, broken into two parts: the First Failure Region (Fig. 4) and the Second Failure Region (Fig. 6). In each case, the optimal shear strength corresponding to the maximum energy absorbed (τ_{opt}) is shown.

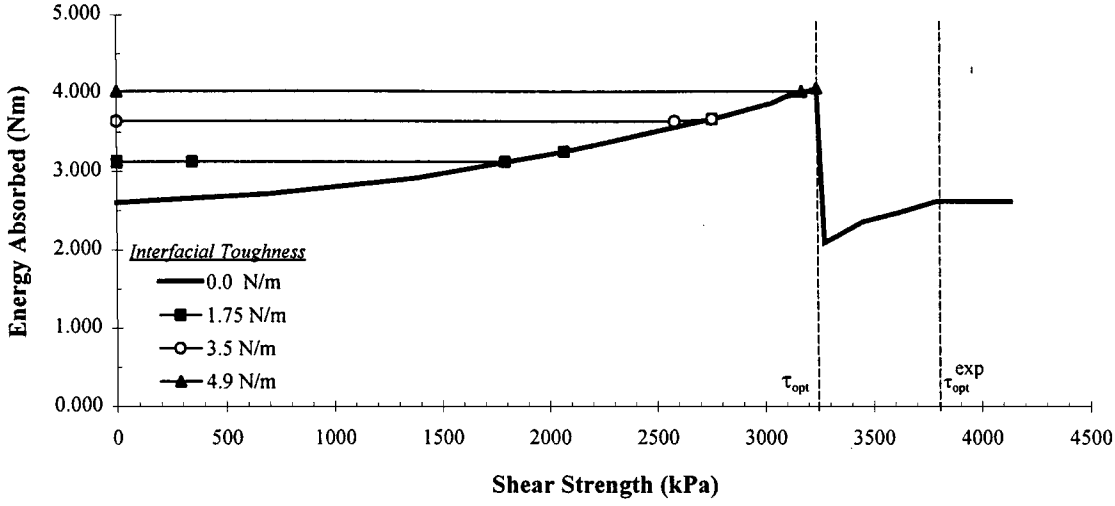

Figure 4 Energy absorbed for $\tau_f \leq \tau_{opt}(h_1 = h_2)$.

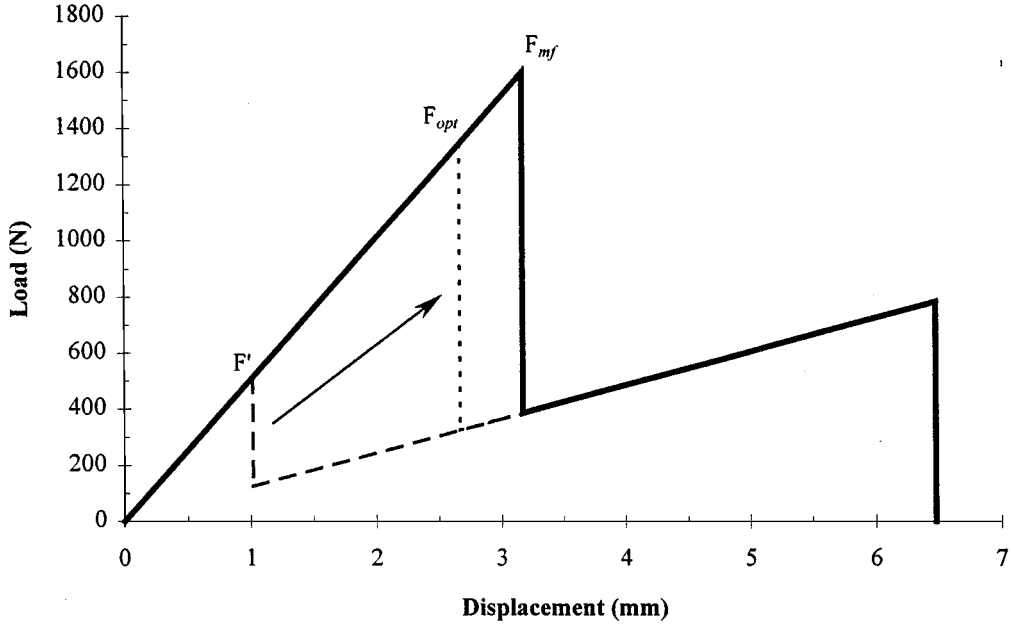

Figure 5 Load-displacement diagram for the first failure region ($h_1 = h_2$).

The First Failure Region includes all points to the left of the discontinuity ($\tau_f \leq \tau_{opt}$) in the Energy vs. Shear Strength plot. By analyzing the data, two basic characteristics were found:

- This region corresponded to complete, unstable delamination of the interface.
- For all values of the shear strength and fracture toughness in this region, the laminate absorbed more energy than a monolithic beam with the same lamina material and geometry.

As long as the shear strength was below the optimal value, increasing the shear strength resulted in a larger first failure load as shown in Fig. 5 ($F' \rightarrow F_{opt}$). Because more of the total energy capacity of the monolithic (unfailed) beam was realized by raising the first failure load, the total energy absorbed also increased.

Since the crack was always found to exhibit unstable propagation, both the shear strength and the fracture toughness controlled not the progression but rather the onset of crack propagation and determined the load at which transition between the undelaminated single layer beam and the completely delaminated two-layer beam occurred (see Fig. 5). Thus, they will both be referred to as delamination or interface control mechanisms.

The baseline plot in Fig. 4 ($G_c = 0.0$ N/m) represents the energy absorbed if the shear strength was the sole delamination control mechanism. When the shear strength was held constant and the interfacial toughness (G_c) was increased, the toughness eventually became the dominant delamination control mechanism. At this point, only an increase in G_c, not τ_f, caused an increase in absorbed energy. When the shear strength was raised enough that it again became the delamination control, the energy absorbed reverted to the baseline. In this case, even though the interface had non-zero toughness, the beam had accumulated so much energy prior to interfacial failure that the fracture toughness was insufficient to resist further crack growth.

The Second Failure Region included all points to the right of the discontinuity ($\tau_f > \tau_{opt}$) in the Energy vs. Shear Strength plot. Again, several characteristics were identified:

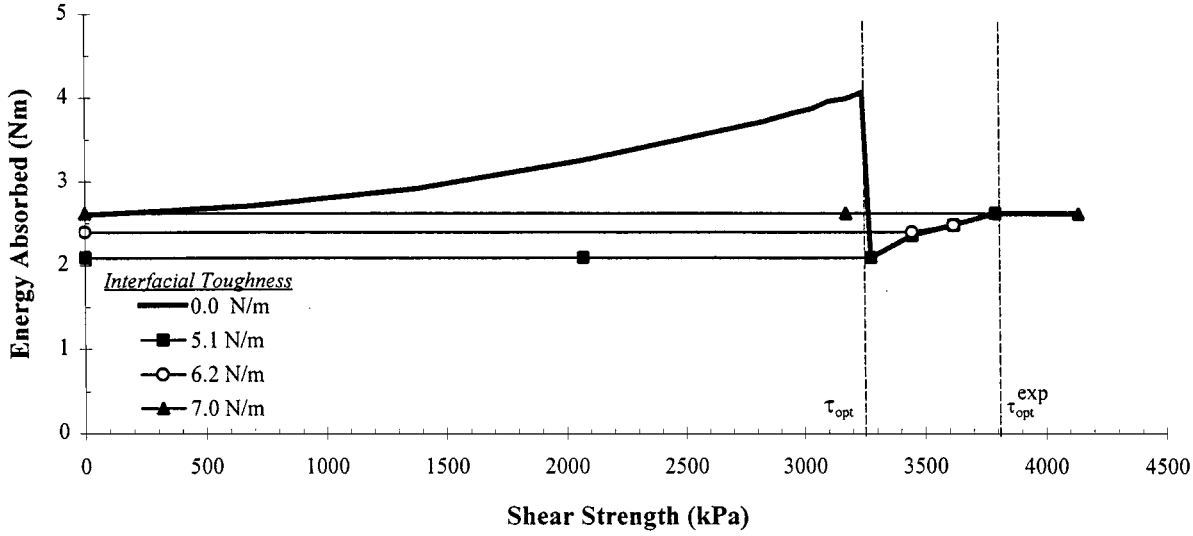

Figure 6 Energy absorbed for $\tau_f > \tau_{opt}(h_1 = h_2)$.

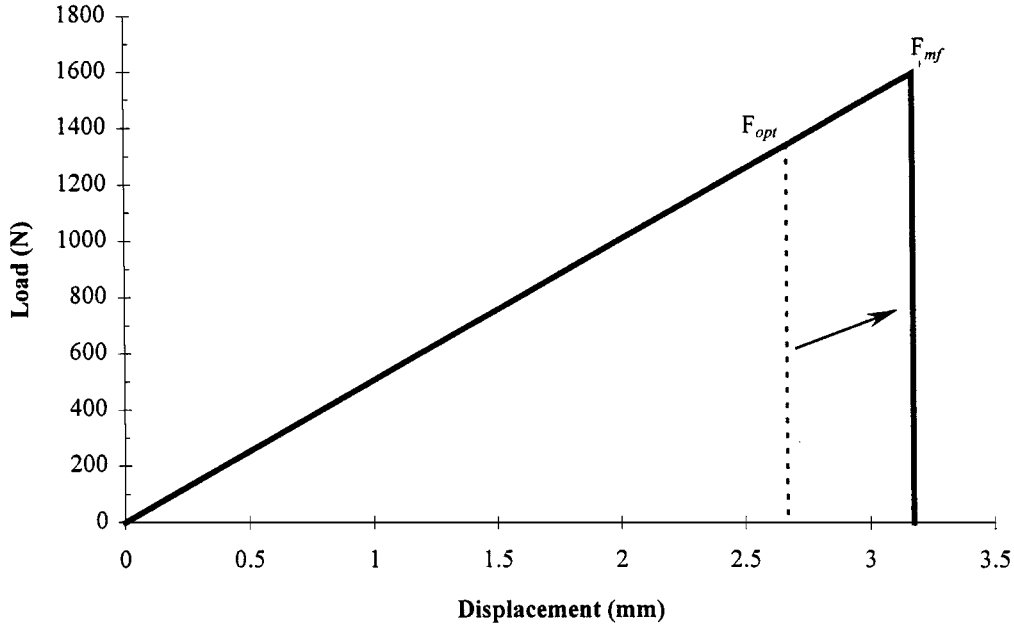

Figure 7 Load-displacement diagram for the second failure region.

- This region corresponded to either incomplete crack propagation or no crack propagation at all.
- For all values of the shear strength and fracture toughness in this region, the laminate absorbed no more (i.e., less than or equal to) energy than a monolithic beam with the same layer material and geometry. Fig. 7 below and proceeding text explain this in more detail.

Since the interface was not allowed to completely fail, the maximum energy possible in this region was that of the monolithic beam. As the shear strength was increased from τ_{opt}, more energy was absorbed until the shear strength at monolithic (tensile) failure, τ_{mf}, was reached (i.e., $F_{opt} \rightarrow F_{mf}$ in Fig. 7). Any increase in τ_f beyond this point resulted in no additional energy absorbed. Thus, for $\tau_{opt} < \tau_f < \tau_{mf}$, the energy absorbed was actually less than that for the monolithic case.

Given these findings, the boundaries of the First and Second Failure Regions may be shown by the G_c vs. τ_f diagram in Fig. 8.

3.2. Theoretical optimal interfacial properties

In order to predict the optimal interfacial strength, a detailed derivation of the laminate's strain energy was performed. Only the key steps are presented here, the remainder may be found in Ref. [10].

A detail of the beam components and their associated forces and moments is given in Fig. 9, below. Since there is no torsion and the beam is two dimensional (i.e., constant width), the strain energy of the structure degenerates to the form given below.

$$U = \int_0^1 \left(\frac{M^2}{EI} + \frac{P^2}{AE} \right) dx \qquad (4)$$

Because of the discontinuity at the crack tip, the integral in Equation 4 must be broken into two parts ($0 \rightarrow a$ and $a \rightarrow 1$), as shown in Fig. 9. In order to simplify the calculation, it is assumed that all three sections are made of the same material (i.e., $E_1 = E_2 = E_3 = E$).

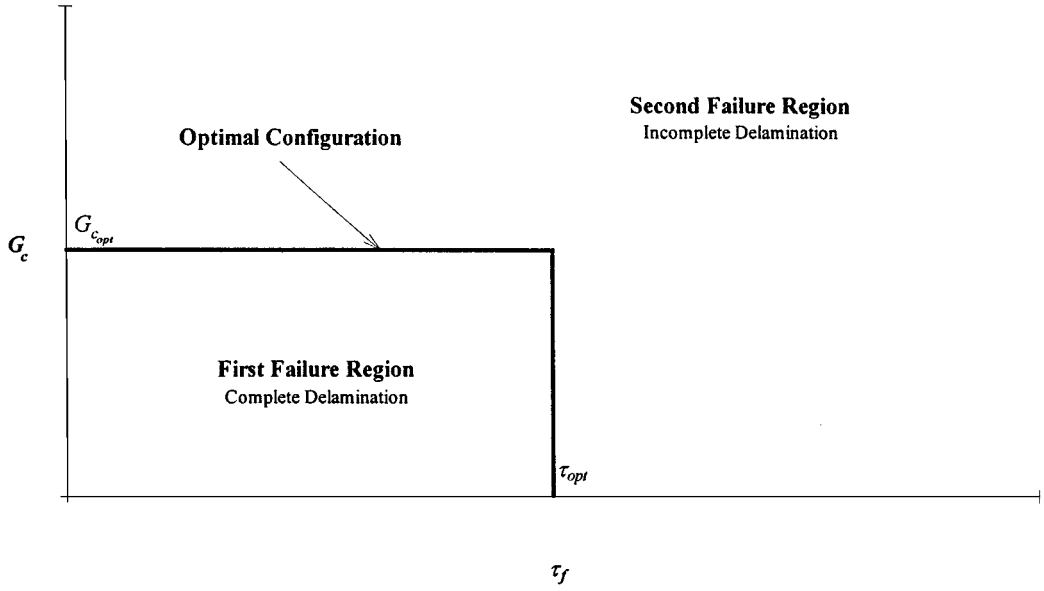

Figure 8 First and second failure regions.

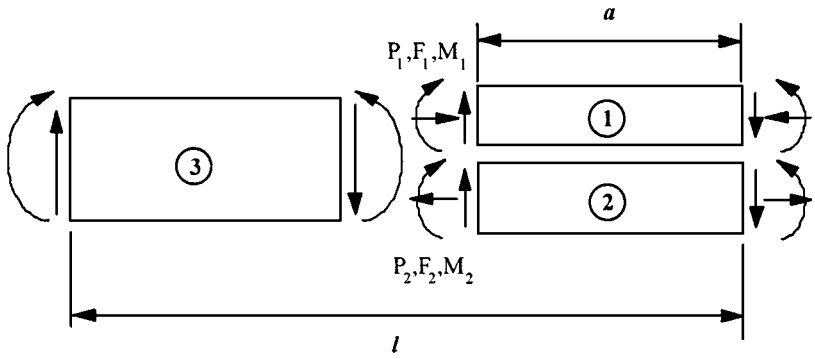

Figure 9 The section loads in a cracked two-layer beam.

Because transverse cracking was not permitted, the vertical displacement of both Sections 1 and 2 must be equal (i.e., $\delta_1 = \delta_2$). Using this result and assuming that both ligaments are considered cantilevers, a simple relationship between the forces and moments in the two layers is found.

$$F_1 = \eta_{1,2} F_2 \qquad M_1 = \eta_{1,2} M_2 \tag{5}$$

where $\eta_{1,2} = h_1^3 / h_2^3$.

Recognizing that the total force and the total moment along the loading line must be the sum of the contributions from the two layers, the final form for the total load and moment along the loading-line is,

$$F = 2(1 + \eta_{1,2}) F_2 \qquad M = 2(1 + \eta_{1,2}) M_2 \tag{6}$$

If the interface constraints are applied, the axial force and the moment in the bottom layer can be found.

$$P = \left(\frac{3}{A_{1,2} + 6B_{1,2}} \right) F_2 (2l - a)$$

$$M_2 = \left(\frac{1}{A_{1,2} + 6B_{1,2}} \right) F_2 l [A_{1,2} - (A_{1,2} + 3B_{1,2})\alpha] \tag{7}$$

Where $\alpha = a/l$, and $A_{1,2}$ and $B_{1,2}$ are both functions of h_1 and h_2.

$$A_{1,2} = \frac{h_2^2}{h_1} \qquad B_{1,2} = \frac{h_1 + h_2}{2(1 + \eta_{1/2})}$$

With Equations 5 and 7, it is possible to express all of the forces and moments, and hence the strain energy, in terms of the vertical load, F. Performing the integration given in Equation 4 and applying Castigliano's theorem gives the final desired result for the combined stress along the bottom layer in terms of the interfacial shear strength.

$$\sigma_2 = \frac{\tau_f L}{12 h_2} \left[\frac{1 + \eta_{1,2}}{\eta_{1,2}^{2/3}(1 + \eta_{1,2}) + 3\eta_{1,2}^{1/3}\left(1 + \eta_{1,2}^{1/3}\right)} \right] \times \left\{ \frac{2\left(1 + \dfrac{1}{\eta_{1,2}^{1/3}}\right) + \left[3\left(\dfrac{1 + \eta_{1,2}^{1/3}}{1 + \eta_{1,2}} \right) - 1 \right] \alpha}{\dfrac{\eta_{1,2}^{1/3}}{4\left(\eta_{1,2}^{1/3} + 1\right)^2} \alpha^3 + \dfrac{1 + \eta_{1,2}}{3\left(\eta_{1,2}^{1/3} + 1\right)^3}} \right\} \tag{8}$$

Maximum stress, and hence failure, will occur in the thickest beam, which in this case was assumed to be the bottom layer (i.e., Layer 2). Since the effect of contact

stresses were neglected, the stress distribution is symmetric and this assumption may be made without any loss of generality.

From Equation 8 the tensile stress is found to be a function of the crack length. Thus, the crack length corresponding to the maximum stress along the loading-line during crack propagation can be found by setting the first derivative of Equation 8 with respect to the crack length to zero. The differentiation produces a very complex solution for $\alpha_{\sigma_{\max}}$. Thus, for the sake of simplicity, the high accuracy curve fit below was used as an approximation.

$$\alpha_{\sigma_{\max}} = \frac{1}{1.5 + 0.7618\eta_{1,2}^{0.3383}} \tag{9}$$

This is the crack length at which the maximum tensile stress along the loading-line occurs. As an example, if $\eta_{1,2} = 1$ (i.e., $h_1 = h_2$), $\alpha_{\sigma_{\max}}$ is at 44.2% of the total beam length. From finite element model data, $\alpha_{\sigma_{\max}}$ was found to be 44.0%.

The optimum shear strength is attained when the tensile stress at $\alpha_{\sigma_{\max}}$ approaches the tensile failure point. Thus, τ_{opt} may be found by substituting Equation 9 into 8 for α with $\sigma_2 = \sigma_{\text{f}}$. This expression is also prohibitively complex, so another curve fit was applied. For greater accuracy, it was broken into two regions based upon the value of $\eta_{1,2}$.

$$\begin{aligned}
&\eta_{1,2} < 0.04\\
&\tau_{\text{opt}} = \left(\frac{0.06985\eta_{1,2}^{0.575629} - 1.8159\cdot 10^{-5}}{\eta_{1,2}^{0.575269} + 0.17935}\right)\\
&\qquad\times\left(\eta_{1,2}^{1/3} + 3\frac{1+\eta_{1,2}^{1/3}}{1+\eta_{1,2}}\right)\sigma_{\text{f}}\frac{h_2}{1}\\
&\eta_{1,2} \geq 0.04\\
&\tau_{\text{opt}} = (0.081275)(1.3415^{\eta_{1,2}})\left(\eta_{1,2}^{0.28244}\right)\\
&\qquad\times\left(\eta_{1,2}^{1/3} + 3\frac{1+\eta_{1,2}^{1/3}}{1+\eta_{1,2}}\right)\sigma_{\text{f}}\frac{h_2}{1}
\end{aligned} \tag{10}$$

Using Equation 1, a similar analysis was conducted for the fracture toughness. With the strain energy in Equation 4, this calculation was trivial and the result is presented below.

$$G_{c_{\text{opt}}} = \left(\eta_{1,2}^{1/3} + 3\frac{1+\eta_{1,2}^{1/3}}{1+\eta_{1,2}}\right)^2 \times\left[\frac{(0.01184)(0.9926353)^{1/\eta_{1,2}}}{\eta_{1,2}^{0.10509434}}\right]\left(\frac{\alpha_0^2\sigma_{\text{f}}^2 h_2}{E}\right) \tag{11}$$

It is important to note that this value is only significant if the beam has already undergone shear failure and the fracture toughness is the primary interface control mechanism.

Additionally, because large errors in the G calculation were encountered at small crack lengths when the Virtual Crack Extension method was used, the optimal value predicted by Equation 11 was generally larger than the finite element result. Since this discrepancy was due to numerical error associated with the forward difference in the Virtual Crack Extension method, the value given by Equation 11 is still considered the theoretically correct one.

4. Design guidelines

Through finite element analysis, four failure modes were identified for two- and three-layered laminates.

1. Monolithic: The laminate failed as a single beam (i.e., no interfacial failure).
2. Single Delamination: Only one of the interfaces completely failed. In the case of the two-layered laminate, this is the only possible interfacial failure mode.
3. Simultaneous Delamination: Both interfaces failed simultaneously.
4. Progressive Delamination: The interfaces failed sequentially and independently.

The failure progression tree for both two- and three-layered laminates is given in Fig. 10. Simultaneous Delamination and Progressive Delamination in the three-layered laminate are designated by dashed and solid lines, respectively.

The stages and their associated symbols (blocks in Fig. 10) demonstrate the crack formation and delamination process. For instance, in a two-layered laminate (Fig. 10a), Stage 1 is the uncracked laminate, Stage 2 is the initial formation of the crack by shear failure, and Stage 3 is the completely delaminated interface. Failure progression from initial crack formation to complete interfacial delamination is permitted because in all stages and all configurations the crack growth occurred unstably. With only one exception (Stage 3) two crack tips are never simultaneously present in the three-layer laminate. Thus, for all other stages, the three-layer laminate may be modeled with the two-layer results.

As long as lamina shear failure is neglected, there are only two possible failure modes in the multi-layered laminate: transverse (tensile) failure and interfacial failure. In order to determine how the laminate failure progresses along the flow diagram in Fig. 10, all of the possible failure loads are calculate at each stage. Depending upon the configuration of the given stage, up to three failure loads are possible: shear failure of the interface (Equation 12), crack propagation along the interface (Equation 13), and tensile failure of the lamina (Equation 14).

$$F_\tau = \frac{b\left[(h_a+h_b)^3 + h_c^3\right]}{3h_a h_b}\tau_{\text{f}} \tag{12}$$

$$F_G = \sqrt{\frac{8Eb^2\left(h_a^3+h_b^3\right)(h_a+h_b)^2}{9h_a h_b a^2\beta^2}}G_{\text{c}} \tag{13}$$

$$F_\sigma = \frac{2b\left(h_a^3+h_b^3+h_c^3\right)}{3Lh_d}\sigma_{\text{f}} \tag{14}$$

The individual loads are calculated using the three formulas given in these equations and the layer thickness

TABLE I Layer thicknesses for the failure stages

Stage	Failure mechanism	Equation	h_a	h_b	h_c	h_d	β
1	Interface 1	12	h_1	$h_2 + h_3$	0		
	Interface 2	12	h_3	$h_1 + h_2$	0		
	Lamina	14	$h_1 + h_2 + h_3$	0	0	$h_1 + h_2 + h_3$	
2	Interface 1	13	h_1	$h_2 + h_3$			1
	Interface 2	12	h_2	h_3	h_1		
	Lamina	14	$\max(h_1, h_2 + h_3)$	$\min(h_1, h_2 + h_3)$	0	$\max(h_1, h_2 + h_3)$	
4	Interface 2	12	h_2	h_3	h_1		
	Lamina	14	$\max(h_1, h_2 + h_3)$	$\min(h_1, h_2 + h_3)$	0	$\max(h_1, h_2 + h_3)$	
5	Interface 2	13	$\max(h_2, h_3)$	$\min(h_2, h_3)$			$1 + \frac{h_1^3}{h_2^3} + \frac{h_1^3}{h_3^3}$
	Lamina	14	h_1	h_2	h_3	$\max(h_1, h_2, h_3)$	
6	Lamina	14	h_1	h_2	h_3	$\max(h_1, h_2, h_3)$	

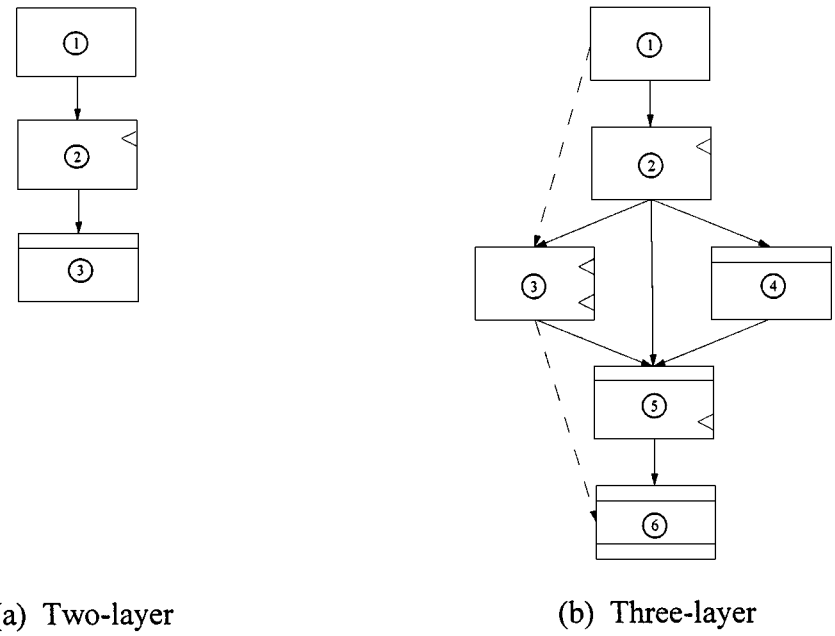

Figure 10 Failure progression in two- and three-layered laminates.

data (Table I) given below. Since no closed-form solutions exist for simultaneous failure (Stage 3), no data is presented for this configuration. Numerical results were found using the finite element model and are presented in Fig. 13. These were used to establish the guidelines in lieu of the closed-form solution.

At every stage, each of these loads are compared. The smallest of which represents the first, and consequently only, failure load for that stage and determines the next stage in the failure progression. There are, however, several special cases.

1. If an interfacial failure is determined to occur, it must be checked against the optimal value for the given stage (Equation 10 for shear failure and Equation 11 for crack propagation). If the failure load exceeds the optimal load then final failure has occurred; otherwise, failure proceeds to the next stage.

2. If the fracture toughness from either Stage 2 or 5 is low compared to the shear strength of the previous stage, it is possible that the load required to continue crack propagation will be lower than the one that initiated shear failure. In this case the interface will fail completely at the shear failure load (i.e., Stage 1 or 4, respectively) and that will be the final load for this stage as well.

3. If any of the interface failure loads for a given stage are equal, then failure occurs simultaneously.

4. For this analysis transverse failure of the lamina was considered catastrophic and, thus, represents a final failure. Transverse failure includes both failure by Equation 14 and violation of the optimal shear strength and interfacial toughness values as described in case 1 above.

This analysis was performed for the entire range of interfacial properties and layer thicknesses. The results from this work were used to determine optimal properties and geometry for both the two- and three-layered laminates. For both configurations, only the shear strength was used as the interface failure control mechanism. Similar numerical tests were run using the fracture toughness as the interfacial failure control mechanism, but the results are not presented here

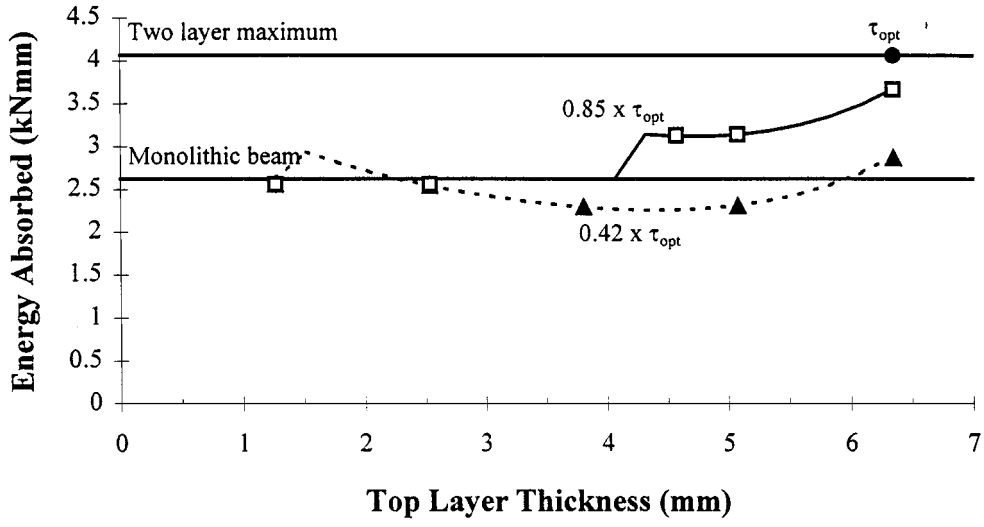

Figure 11 Optimal energy absorption for a two-layered beam with shear strength.

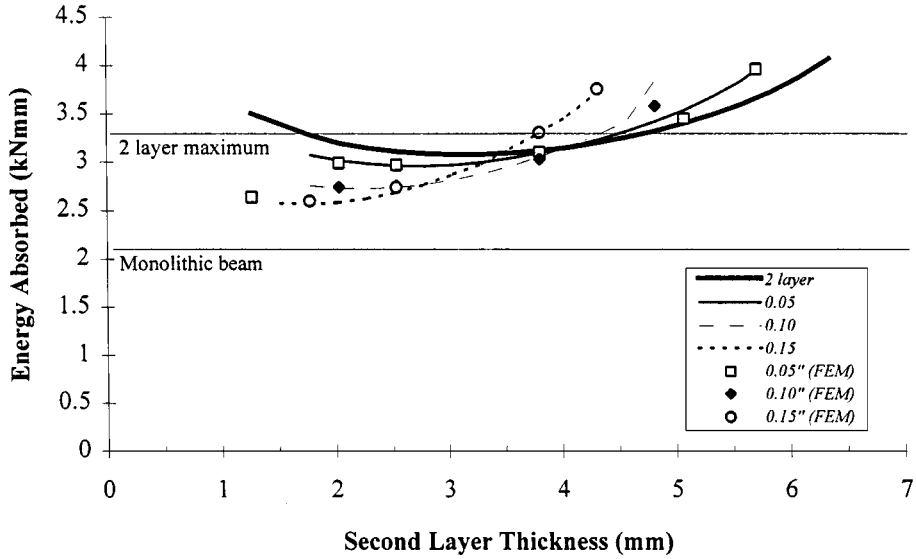

Figure 12 Optimal energy absorption for progressive failure in a three-layered laminate.

because they exhibited the same trend and provided no additional information. Finite element results were used to verify the data at discrete points in Figs 11 and 12 (denoted by the data symbols).

4.1. Two-layered laminate

For the two-layered laminate, each of the layer thicknesses and the interface shear strength were varied while the total thickness was held constant. The simulated laminates were loaded until tensile failure and the results are shown in Fig. 11. This figure shows the total energy absorbed by the beam for a given top layer thickness (total beam thickness is 1/2 in.). Total energy was found by integrating the force-displacement diagram.

The Monolithic Beam line is the energy absorbed by a single layered beam of equivalent total thickness, and the two-layer maximum is the maximum energy absorbed by a two-layered laminate. The sudden drop in energy absorption on the left portion of the 42% τ_{opt} and 85% τ_{opt} curves marked the transition from monolithic failure to complete interfacial delamination. The value for τ_{opt} was obtained through Equation 10.

It was immediately apparent from Fig. 11 that equal thickness layers produced the best energy absorption in two-layered beams. As the optimal shear strength was approached the energy curve shifted vertically and the failure mode transition point shifted to the right until the two-layer maximum was reached. As long as the interface properties and layer thicknesses may be controlled such that optimal values are available, this is the desired configuration. The 42% τ_{opt} and 85% τ_{opt} curves in Fig. 14 also demonstrated that when laminates are employed, the energy absorbed can actually be less than that of a monolithic beam. Thus, great care must be exercised in the selection of the interfacial properties and the laminate configuration.

4.2. Three-layered laminate

As with the two-layered laminates, the layer thicknesses were varied from 0 to 50% of the total thickness. For progressive delamination (Fig. 12), the criteria established in the two-layer laminate theories were used to determine the optimal shear strength at each stage (see Fig. 10) and the corresponding the amount of energy absorbed. Due to the presence of the second crack tip

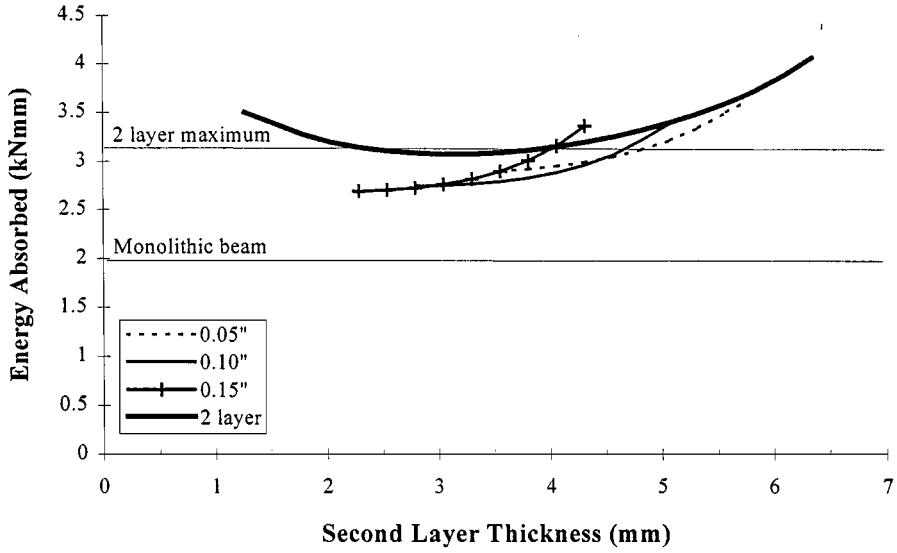

Figure 13 Optimal energy absorption for simultaneous failure in a three-layered laminate.

in Stage 3, no closed form solutions for the optimal interfacial properties and failure loads were found for simultaneous failure. In this case, an iterative procedure employing the finite element model was used. Graphs of both analyses are shown in Figs 12 and 13. In each case, the two-layered data is also given for comparison. Fig. 12 was generated using the closed-form results and several finite element data points are shown as verification. Fig. 13 was created by repeated runs of the finite element model since, as stated previously, no closed form solutions exist for this case.

In both modes it appears that the two-layer case was a maximum and that, as the top layer thickness decreased, the three-layered results approached this maximum. Thus, as $h_1 \to 0$, $E^{\text{3-layer}}_{\text{absorbed}} = E^{\text{2-layer}}_{\text{absorbed}}$. It is believed that not permitting transverse tensile failure of the lamina is the probable cause of this result. If the individual layers were allowed to crack transversely as in [11], it is likely that the three-layered laminate would have been more energy absorbent. Thus, if delamination is the only failure mechanism permitted and optimum interfacial materials are available, the two-layered laminate with equal thickness layers is the optimal configuration.

It is important to note that this analysis is very sensitive to the in-plane shear stress distribution used in determining interlaminar shear failure. It appears that the optimal case is one in which the interface lies along the point of maximum shear. With a parabolic shear distribution, the optimal condition will result if the interface is along the middle of the beam (i.e., equal thickness layers). When contact stresses are considered, the distribution is no longer parabolic and the point of maximum shear will shift toward the point of application of the load. Thus, it is likely that equal thickness layers will not be optimum. Further work accounting for the contact stress distributions needs to be done to verify this result.

5. Conclusions

A detailed study of the mechanics of energy absorption by delamination in layered materials was performed using finite element methods. Prompted by the results of this analysis, closed from solutions were found for the optimal shear strength and the optimal fracture toughness for the interface of a two-layered laminate. The results were then used to develop design guidelines for improved energy absorption for both two- and three-layered laminates.

The major findings of this work are:

- The tensile stresses along the midplane during delamination are nonlinear and attain a maximum at some crack length, $\alpha_{\sigma_{\max}}$.
- The optimal interfacial strengths (shear and fracture toughness) for a two-layered laminate in which transverse failure is inhibited were determined and are presented in Equations 10 and 11, respectively.
- Using failure branching criteria, the energy absorbed by both a two- and a three-layered laminate prior to tensile failure was found. Based upon these guidelines, the optimal energy absorption configuration was found to be a two-layer beam with equal thickness layers as long as interface materials are available such that $\tau_f = \tau_{\text{opt}}$ and $G_c \leq G_{c_{\text{opt}}}$ or $G_c = G_{c_{\text{opt}}}$ and $\tau_f \leq \tau_{\text{opt}}$. These interfacial properties were the largest values that still permitted complete delamination. If the properties are not optimal, it is possible that another geometric configuration could give maximum energy absorption, although this energy will still be less than that achieved with optimal materials. The design guidelines provided should assist in determining the correct geometry.

References

1. VAAMONDE, A. J. VÁZQUEZ, *Journal de Physique* **3**(7) (1993) 773–781.
2. C. T. SUN and T. L. NORMAN, *Composites Science and Technology* **39** (1990) 327–340.
3. S. A. HITCHEN and R. M. KEMP, *Composites* **26** (1995) 207–214.
4. B. TISSINGTON, G. POLLARD and I. M. WARD, *Composites Science and Technology* **44** (1992) 197–208.

5. Y. S. KWON and B. V. SANKAR, Indentation-Flexure and Low-Velocity Impact in Graphite/Epoxy Laminates. NASA Contractor Report 187624, March 1992.
6. A. A. GRIFFITH, *Philosophical Trans. of the Royal Soc. of London* **A221** (1921) 163–198.
7. J. R. RICE, *J. Appl. Mech.* **35** (1968) 379–386.
8. B. V. SANKAR, *Computers & Structures* **38**(2) (1991) 239–246.
9. B. V. SANKAR and V. SONIK, *AIAA Journal* **33**(7) (1996) 1312–1318.
10. M. H. LEAR, "Mechanics of Delamination Growth in Multi-Layered Materials Under Low-Velocity Impact." Appendix B, May 1996.
11. A. J. PHILLIPPS, W. J. CLEGG and T. W. CLYNE, *Acta. Metall. Mater.* **41**(3) (1993) 805–827.

Received 22 September
and accepted 11 November 1998